STRUCTURAL CHEMISTRY
ISSN 2053-2296

Synthesis, crystal structure and studies on the interaction with albumin of a new silver(I) complex based on 2-(4-nitrobenzenesulfonamido)benzoic acid

Lucius Flavius Ourives Bomfim Filho, Cleidivania Rocha, Bernardo Lages Rodrigues,* Heloisa Beraldo and Leticia Regina Teixeira*

Chemistry Department, Universidade Federal de Minas Gerais, 31270-901 Belo Horizonte, Minas Gerais, Brazil. *Correspondence e-mail: bernardo@qui.ufmg.br, lreginaufmg@gmail.com

Received 10 April 2019
Accepted 17 June 2019

Edited by B. D. Santarsiero, University of Illinois at Chicago, USA

Keywords: coordination polymer; crystal structure; silver complex; sulfonamide; Hirshfeld surface; human serum albumin.

CCDC references: 1934725; 1934724

Supporting information: this article has supporting information at journals.iucr.org/c

In the present work, the two-dimensional (2D) polymer poly[[μ_4-2-(4-nitrobenzenesulfonamido)benzoato-$\kappa^4O^1{:}O^1{:}O^{1'}{:}N^6$]silver(I)] (Ag*L*), $[Ag(C_{13}H_9N_2O_6S)]_n$, was obtained from 2-(4-nitrobenzenesulfonamido)benzoic acid (H*L*), $C_{13}H_{10}N_2O_6S$. FT–IR, ^{1}H and $^{13}C\{^1H\}$ NMR spectroscopic analyses were used to characterize both compounds. The crystal structures of H*L* and Ag*L* were determined by single-crystal X-ray diffraction. In the structure of H*L*, O—H···O hydrogen bonds between neighbouring molecules result in the formation of dimers, while the silver(I) complex shows polymerization associated with the O atoms of three distinct deprotonated ligands (L^-). Thus, the structure of the Ag complex can be considered as a coordination polymer consisting of a one-dimensional linear chain, constructed by carboxylate bridging groups, running parallel to the *b* axis. Neighbouring polymeric chains are further bridged by Ag—C monohapto contacts, resulting in a 2D framework. Fingerprint analysis of the Hirshfeld surfaces show that O···H/H···O hydrogen bonds are responsible for the most significant contacts in the crystal packing of H*L* and Ag*L*, followed by the H···H and O···C/C···O interactions. The Ag···Ag, Ag···O/O···Ag and Ag···C/C···Ag interactions in the Hirshfeld surface represent 12.1% of the total interactions in the crystal packing. Studies of the interactions of the compounds with human serum albumin (HSA) indicated that both H*L* and Ag*L* interact with HSA.

1. Introduction

The rational design and construction of metal–organic coordination polymers has attracted considerable interest due to their fascinating topologies and the promising applications of these compounds as luminescence (Pan *et al.*, 2018; Feng *et al.*, 2015) and magnetic probes (Chen *et al.*, 2016), in the degradation of organic pollutants (Wu *et al.*, 2015) and as antimicrobial agents (Roca *et al.*, 2016). The Ag^I ion has a very flexible coordination sphere, supporting variable coordination numbers from two to six and numerous geometries, ranging from linear all the way to octahedral (Yang *et al.*, 2017). This makes coordination to Ag^I an interesting strategy for obtaining new metal–organic coordination polymers.

Silver(I) complexes and nanoparticles present a wide range of applications. Silver compounds show antimicrobial, anti-inflammatory and antiviral activities (Santos *et al.*, 2018; Guldiren & Aydin, 2017; Hussaini *et al.*, 2019) and are employed in ointments for burns (Hussain & Ferguson, 2006). Carboxylic acids have been shown to be good building blocks for the constructuion of diverse coordination polymers (Li *et al.*, 2006). 4-Aminobenzoic acid presents interesting poly-

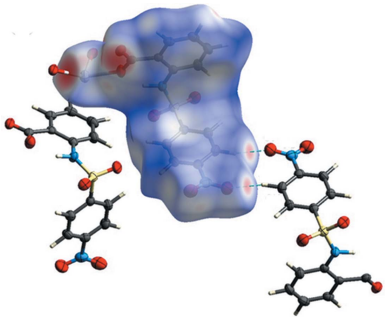

morphism (Rosbottom *et al.*, 2018) and numerous biological activities (Prior *et al.*, 2014; Igberase *et al.*, 2019). In a previous work, we reported the syntheses of 4-(2-nitrobenzenesulfonamido)benzoic acid and its tri-*n*-butyltin(IV) complex (Bomfim Filho *et al.*, 2019).

Studies on the interactions of small molecules and proteins may provide important information about the binding mechanism, binding constants and interaction sites. Human serum albumin (HSA) is the most abundant protein in human blood plasma (*ca* 60%), being involved in the distribution, metabolism and elimination of drugs (Ascenzi *et al.*, 2014). It has been shown that silver(I) complexes with a variety of organic ligands bind to HSA (Yilmaz *et al.*, 2017) and to bovine serum albumin (BSA) (Tamayo *et al.*, 2017), suggesting that the complexes could be transported by albumins.

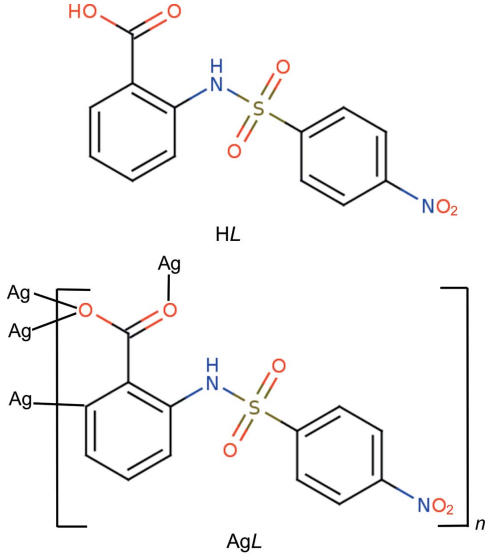

Scheme 1

In the present work, we used 2-(4-nitrobenzenesulfonamido)benzoic acid (H*L*) (Fig. 1) to obtain a new silver(I) complex (Ag*L*) (see Scheme 1). The crystal structures of both were determined by single-crystal X-ray diffraction. The Hirshfeld surfaces were used to describe the intermolecular interactions. In addition, the interaction of the compounds with HSA was investigated by steady-state fluorescence spectroscopy.

2. Experimental

The reactants were purchased from Sigma–Aldrich and used without further purification. Melting points were determined using an MQAPF-302 apparatus and are reported without correction. NMR spectra were recorded on a Bruker Avance DRX-400 spectrometer in hexadeuterodimethyl sulfoxide (DMSO-d_6) with tetramethylsilane (TMS) as an internal standard. The IR spectra were recorded on a PerkinElmer FT–IR GX spectrophotometer using KBr pellets. Electronic spectra were recorded on a Shimadzu UV-2401PC UV–Vis spectrophotometer using a 1.0 cm beam-path quartz cuvette. Steady-state fluorescence measurements were performed on a Varian–Agilent Cary Eclipse Fluorescence Spectrophotometer (L1006m016, Agilent Technologies) also using a 1.0 cm quartz cell.

2.1. Synthesis and crystallization

2.1.1. Synthesis of 2-(4-nitrobenzenesulfonamido)benzoic acid (H*L*). The synthesis followed a procedure described in the literature (Deng & Mani, 2006). Stoichiometric amounts of 4-nitrobenzenesulfonyl chloride and 2-aminobenzoic acid were suspended in distilled water (100 ml). Under vigorous stirring, an aqueous solution of sodium carbonate was added to adjust the pH to between 8.0 and 9.0. After the consumption of the reagents and stabilization of the pH, concentrated HCl solution was added to attain a pH of 2.0, which allowed precipitation of H*L*. The solid was filtered off, washed with water to remove excess HCl and dried *in vacuo*. Single crystals suitable for X-ray analysis were obtained by slow evaporation from an ethanol solution.

Analytical and spectroscopic data: yield (%) 81; m.p. 227–229 °C. Analysis calculated (%) for $C_{13}H_{10}N_2O_6S$: C 47.89, H 3.07, N 8.53; found: C 48.45, H 3.13, N 8.69. FT–IR (selected bands) (KBr pellet, cm^{-1}): ν(N—H) 3100, ν(C=O) 1666, δ(N—H) 1582, $\nu_{as}(NO_2)$ 1530, $\nu_{as}(SO_2)/\nu_s(NO_2)$ 1348, ν(C—O) 1264, $\nu_s(SO_2)$ 1178, ν(S—N) 926. ^{1}H NMR (400 MHz, DMSO-d_6, ppm): δ_H 11.30 (*s*, 1H, NH), 8.36 (*d*, ^3J = 8.8 Hz, 1H, H9/H13), 8.06 (*d*, ^3J = 8.7 Hz, 2H, H10/H12), 7.90 (*d*, ^3J = 7.2 Hz, 1H, H7), 7.65–7.44 (*m*, 2H, H4/H5), 7.18 (*t*, *J* = 7.1 Hz, 1H, H6). ^{13}C NMR (100 MHz, DMSO-d_6, ppm): δ_C 169.4 (C1), 150.1 (C11), 144.1 (C8), 138.7 (C3), 134.5 (C5), 131.6 (C7), 128.5 (C10/C12), 124.7 (C9/C13), 124.1 (C6), 119.3 (C4), 117.9 (C2).

2.1.2. Synthesis of Ag*L*. To an ethanol solution (40 ml) containing H*L* (1.0 mmol) was added dropwise an aqueous solution of NaOH to adjust the pH of the solution to 7.0. After an hour of stirring, an aqueous solution of $AgNO_3$ (1.0 mmol) was added. The reaction mixture was stirred in the dark at room temperature for a further 24 h. The resulting solid was filtered off and washed with water, ethanol and diethyl ether, and dried *in vacuo*. Single crystals suitable for X-ray analysis were obtained by slow evaporation from the mother solution stored in the dark at 298 K.

Analytical and spectroscopic data: yield (%) 63; m.p. 165.2 °C (decomposition). Analysis calculated (%) for $C_{13}H_9AgN_2O_6S$: C 36.36, H 1.80, N 6.58; found: C 36.38, H 2.11, N 6.53. FT–IR (selected bands) (KBr pellet, cm^{-1}): ν(N—H) 3106, ν_{as}(COO) 1608, $\nu_{as}(NO_2)$ 1530, $\nu_{as}(SO_2)/\nu_s(NO_2)$ 1374/1348, ν_s(COO) 1284, $\nu_s(SO_2)$ 1164, ν(S—N) 942, ν(Ag—O) 536. ^{1}H NMR (400 MHz, DMSO-d_6, ppm): δ_H 8.29 (*d*, ^3J = 8.7 Hz, 1H, H9/H13), 7.99 (*d*, ^3J = 8.7 Hz, 2H, H10/H12), 7.88 (*d*, ^3J = 7.7 Hz, 1H, H7), 7.38 (*d*, ^3J = 8.2 Hz, 1H, H4), 7.27 (*t*, ^3J = 7.7 Hz, 1H, H5), 6.88 (*t*, ^3J = 7.5 Hz, 1H, H6). ^{13}C NMR (100 MHz, DMSO-d_6, ppm): δ_C 169.6 (C1), 149.3 (C11), 147.3 (C8), 142.9 (C3), 132.1 (C5), 131.4 (C7), 127.9 (C10/C12), 124.4 (C9/C13), 121.4 (C2), 120.9 (C4), 117.6 (C6).

2.2. Crystal structure determination

Crystal data, data collection and structure refinement details are summarized in Table 1. The H atom of the sul-

Table 1
Experimental details.

Experiments were carried out with Mo $K\alpha$ radiation using a Rigaku Xcalibur Atlas Gemini ultra diffractometer. Absorption was corrected for by multi-scan methods (*CrysAlis PRO*; Rigaku OD, 2018). H-atom parameters were constrained.

	H*L*	Ag*L*
Crystal data		
Chemical formula	$C_{13}H_{10}N_2O_6S$	$[Ag(C_{13}H_9N_2O_6S)]$
M_r	322.29	429.15
Crystal system, space group	Triclinic, $P\overline{1}$	Monoclinic, $P2_1/c$
Temperature (K)	301	293
a, b, c (Å)	6.9140 (3), 10.0641 (5), 10.1532 (5)	19.9216 (7), 5.2391 (2), 13.0860 (4)
α, β, γ (°)	102.153 (4), 100.951 (4), 99.745 (4)	90, 91.864 (3), 90
V (Å^3)	661.77 (6)	1365.08 (8)
Z	2	4
μ (mm^{-1})	0.28	1.67
Crystal size (mm)	0.68 × 0.35 × 0.14	0.21 × 0.18 × 0.17
Data collection		
T_{min}, T_{max}	0.901, 1.000	0.601, 1.000
No. of measured, independent and observed [$I > 2\sigma(I)$] reflections	13718, 4515, 3841	22926, 3553, 2723
R_{int}	0.043	0.046
$(\sin\theta/\lambda)_{max}$ (Å^{-1})	0.761	0.693
Refinement		
$R[F^2 > 2\sigma(F^2)]$, $wR(F^2)$, S	0.041, 0.116, 1.06	0.037, 0.082, 1.07
No. of reflections	4515	3553
No. of parameters	200	208
$\Delta\rho_{max}$, $\Delta\rho_{min}$ (e Å^{-3})	0.33, −0.37	0.82, −0.78

Computer programs: *CrysAlis PRO* (Rigaku OD, 2018), *SHELXS97* (Sheldrick, 2008), *SHELXL2018* (Sheldrick, 2015) and *Mercury* (Macrae *et al.*, 2008).

fonamide group was located in a difference Fourier map and fixed to the parent atom, with N—H = 0.86 Å and U_{iso}(H) = 1.2U_{eq}(N). The other H atoms were fixed geometrically considering the hybridization of the parent atom, with U_{iso}(H) = 1.5U_{eq}(O) and 1.2U_{eq}(C).

2.3. Hirshfeld surface analysis

Hirshfeld surfaces and the associated two-dimensional (2D) fingerprint plots were generated for the crystal structures using *CrystalExplorer* (Version 17.5; Spackman & Jayatilaka, 2009; Spackman & McKinnon, 2002; Turner *et al.*, 2017). The 3D d_{norm} surfaces were mapped over a fixed colour scale of −0.600 (red) to +1.200 a.u. (blue). The 2D fingerprint plots were generated using the translated 0.4–3.0 Å range, including reciprocal contacts.

2.4. Studies on the interactions of H*L* and Ag*L* with HSA

A stock solution of HSA was prepared by dissolving the desired amount of HSA in an 8.3 mmol l^{-1} Tris-HCl buffer at pH 7.2 (Na^+ = 83 mmol l^{-1}). The solutions were first prepared using dimethyl sulfoxide (DMSO) as co-solvent, and then diluted with a Tris-HCl buffer (pH 7.2). All fluorescence spectra were measured after 5 min of incubation.

The fluorescence emission spectra were measured at 298 K using an excitation wavelength of 295 nm and an emission wavelength in the 305–550 nm range, with excitation and emission slits set at 10 nm. The HSA UV–Vis spectra were measured at 298 K in the 200–300 nm range. The HSA concentration was kept constant at 2.38 × 10^{-6} mol l^{-1}, while the H*L* and Ag*L* concentrations ranged from 0 to 5.71 × 10^{-6} mol l^{-1}. Protein concentration was determined by optical density measurements at 280 nm using the molar absorption coefficient (ε) value at this wavelength (35 353 M^{-1} cm^{-1}).

The interactions of H*L* and Ag*L* with HSA were investigated by monitoring the fluorescence quenching of the tryptophan residue (Trp-214). The quenching plot was obtained by the Stern–Volmer Equation (1):

$$F/F_0 = 1 + K_{SV}[Q] = 1 + k_q\tau_0[Q], \quad (1)$$

where F and F_0 are the fluorescence intensities of HSA in the presence and absence of the compounds, respectively, K_{SV} is the Stern–Volmer quenching constant, k_q is the bimolecular quenching rate constant, τ_0 (~10^{-8}) is the lifetime in the absence of quencher and $[Q]$ is the quencher concentration (Lakowicz & Weber, 1973). The binding constant (K_b), the number of binding sites in compound–HSA (η) and the change in free energy (ΔG) were calculated using Equations (2) and (3):

$$\ln\left[(F_0/F) - 1\right] = \ln(K_b) + \eta\ln[Q], \quad (2)$$

$$\Delta G = -RT\ln(K_b), \quad (3)$$

where K_b is the binding constant at the corresponding temperature, R = 8.31 J mol^{-1} K^{-1} is the universal gas constant and T is the temperature in Kelvin. To eliminate any inner-filter effect arising from UV–Vis absorption, the fluorescence data were corrected according Equation (4):

$$F = F_{measured} \times 10^{\left[(A_{em}+A_{exc})/2\right]}, \quad (4)$$

where F is the corrected fluorescence intensity, $F_{measured}$ is the measured fluorescence intensity and A_{exc} and A_{em} are the

Table 2
Selected bonds lengths (Å) and angles (°).

	H*L*	Ag*L*
O1—C1	1.3128 (15)	1.260 (3)
O2—C1	1.2368 (16)	1.256 (3)
S1—O3	1.4293 (10)	1.426 (2)
S1—O4	1.4271 (10)	1.429 (2)
S1—N1	1.6287 (11)	1.624 (2)
S1—C8	1.7733 (12)	1.768 (3)
O5—N2	1.2226 (16)	1.214 (4)
O6—N2	1.2232 (16)	1.226 (4)
N1—C3	1.4109 (16)	1.395 (4)
N2—C11	1.4742 (16)	1.476 (4)
C1—C2	1.4745 (17)	1.504 (4)
Ag1—O1^{i}		2.290 (2)
Ag1—O1^{ii}		2.437 (2)
Ag1—O2		2.304 (2)
Ag1—C6		2.551 (3)
Ag1—Ag1^{i}		3.2926 (3)
O3—S1—O4	120.22 (6)	120.67 (14)
O3—S1—N1	104.49 (6)	103.59 (13)
O4—S1—N1	109.78 (6)	109.82 (14)
O3—S1—C8	108.39 (6)	108.40 (14)
O4—S1—C8	107.11 (6)	107.19 (14)
N1—S1—C8	106.03 (6)	106.35 (13)
C3—N1—S1	126.42 (8)	130.8 (2)
O1^{i}—Ag1—O2		111.09 (8)
O1^{i}—Ag1—O1^{ii}		124.83 (6)
O2—Ag1—O1^{ii}		99.39 (8)
O1^{i}—Ag1—C6		104.70 (9)
O2—Ag1—C6		128.72 (10)
O1^{ii}—Ag1—C6		88.52 (9)

Symmetry codes: (i) $-x+1, y+\frac{1}{2}, -z+\frac{1}{2}$; (ii) $x, y+1, z$.

measured absorbances at the excitation and emission wavelengths, respectively.

3. Results and discussion

3.1. Spectroscopic analysis

The FT–IR spectrum of H*L* shows three common features associated with the carboxylic acid group: a band attributed to ν(O—H) in the 3300–2500 cm^{-1} range and two bands attributed to ν(C═O) and ν(C—O) at 1666 and 1264 cm^{-1}, respectively. For Ag*L*, the presence of two bands at 1608 and 1284 cm^{-1} was attributed to the asymmetric and symmetric stretching vibration modes of the carboxylate group, respectively. $\Delta\nu = \nu_{as}(COO) - \nu_{s}(COO)$ was found to be 324 cm^{-1}, which is characteristic of anisobidentate coordination (Nakamoto, 2008).

The sulfonamide group presents a narrow band related to the ν(N—H) stretching vibration in the 3106–3100 cm^{-1} range. In addition, an angular deformation vibration δ(N—H) at 1582 cm^{-1} is observed in the H*L* spectrum, which is overlapped with the ν_{as}(COO) vibration in the spectrum of the complex. In addition, two bands in the 1374–1348 and 1178–1164 cm^{-1} ranges were attributed to the S═O asymmetric and symmetric stretching vibration modes, respectively. The $\nu_{as}(NO_2)$ mode was found at 1530 cm^{-1} in both compounds. The $\nu_{s}(NO_2)$ band overlapped with the $\nu_{as}(SO_2)$ vibration was observed at 1348 cm^{-1} in H*L* and at 1374 cm^{-1} in Ag*L*. Moreover, an absorption at 467 cm^{-1} in the spectrum of the complex was attributed to the ν(AgO) mode, indicating that the ligand is attached to the Ag^{I} centre through a carboxylate O atom (Nakamoto, 2008).

The ^{1}H NMR spectrum of H*L* shows a singlet at 11.30 ppm attributed to the sulfonamide N—H group, which is absent in the complex. The signals of the aromatic H atoms, mainly the atoms of the aminobenzoic acid group, which are next to the complexation binding site, observed at δ_H 7.18–8.36 in H*L*, undergo significant shifts to δ_H 6.88–8.29 ppm in the complex. The ^{13}C{^{1}H} NMR also shows shifts of the carbon signals in the complex relative to their positions in the free ligand, in particular, the upfield shift of the C6—H6 signals at δ_H 7.18 and δ_C 124.1 in the free ligand to δ_H 6.88 and δ_C 117.6 after complexation. This shift is explained by the monohapto interaction of Ag^{I} with atom C6, as confirmed by the crystal structure analysis.

3.2. Structure description

H*L* crystallized in the triclinic space group $P\overline{1}$, with one molecule per asymmetric unit, while Ag*L* crystallizes in the monoclinic space group $P2_1/c$, with the asymmetric unit formed by one Ag^{I} ion and one monoanionic L^{-} ligand (Fig. 1).

H*L* presents characteristic C═O [1.2368 (16) Å] and C—O [1.3128 (15) Å] bond lengths. For Ag*L*, the carboxylate group presents C—O bond lengths intermediate between single and double bonds, with C1═O1 = 1.260 (3) Å and C2═O2 =

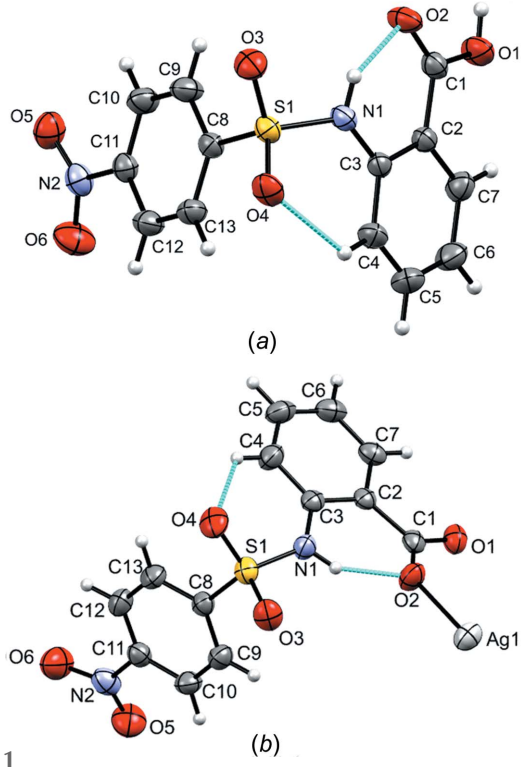

Figure 1
View of the asymmetric units of (*a*) H*L* and (*b*) Ag*L*, showing the atom-numbering schemes used for the NMR characterization. Displacement ellipsoids are drawn at the 50% probability level. Intramolecular hydrogen bonds are represented by blue dashed lines.

1.256 (3) Å (Table 2). The bond lengths of the sulfonamide group (formed by the N1, S1, O3, O4 and C8 atoms) do not change after complexation, similar to the bond lengths of the NO_2 group. In addition, both compounds show equivalent S═O sulfonyl bond lengths, in good agreement with the literature (Shakuntala *et al.*, 2017). The sulfonamide group presents a distorted tetrahedral arrangement around the S atom (Table 2).

In H*L*, the carboxylic acid group is coplanar with aromatic ring *A* (atoms C2–C7), with a dihedral angle of 1.1 (1)° between the planes, while in the complex, the carboxylate group is rotated by 10.8 (2)° from the mean plane through aromatic ring *A*. On the other hand, the nitro group is rotated from the mean plane of aromatic ring *B* (atoms C8–C12), with a dihedral angle of 15.3 (2)° in H*L* and 13.4 (1)° in Ag*L*.

The crystal structures of H*L* and Ag*L* present two intramolecular hydrogen bonds each, *viz.* N1—H1N···O2 [N1···O2 = 2.6559 (14) Å for H*L* and 2.602 (3) Å for Ag*L*] and C4—H4···O4 [C4···O4 = 3.0729 (18) Å for H*L* and 3.062 (4) Å for Ag*L*]. These hydrogen bonds reduce the free rotation at the C1—C2 and N1—S1 single bonds, generating two *S*(6) rings (Fig. 1).

The characteristic dimer formation by the intermolecular O1—H1···O2^{i} hydrogen bonds and the weak intermolecular

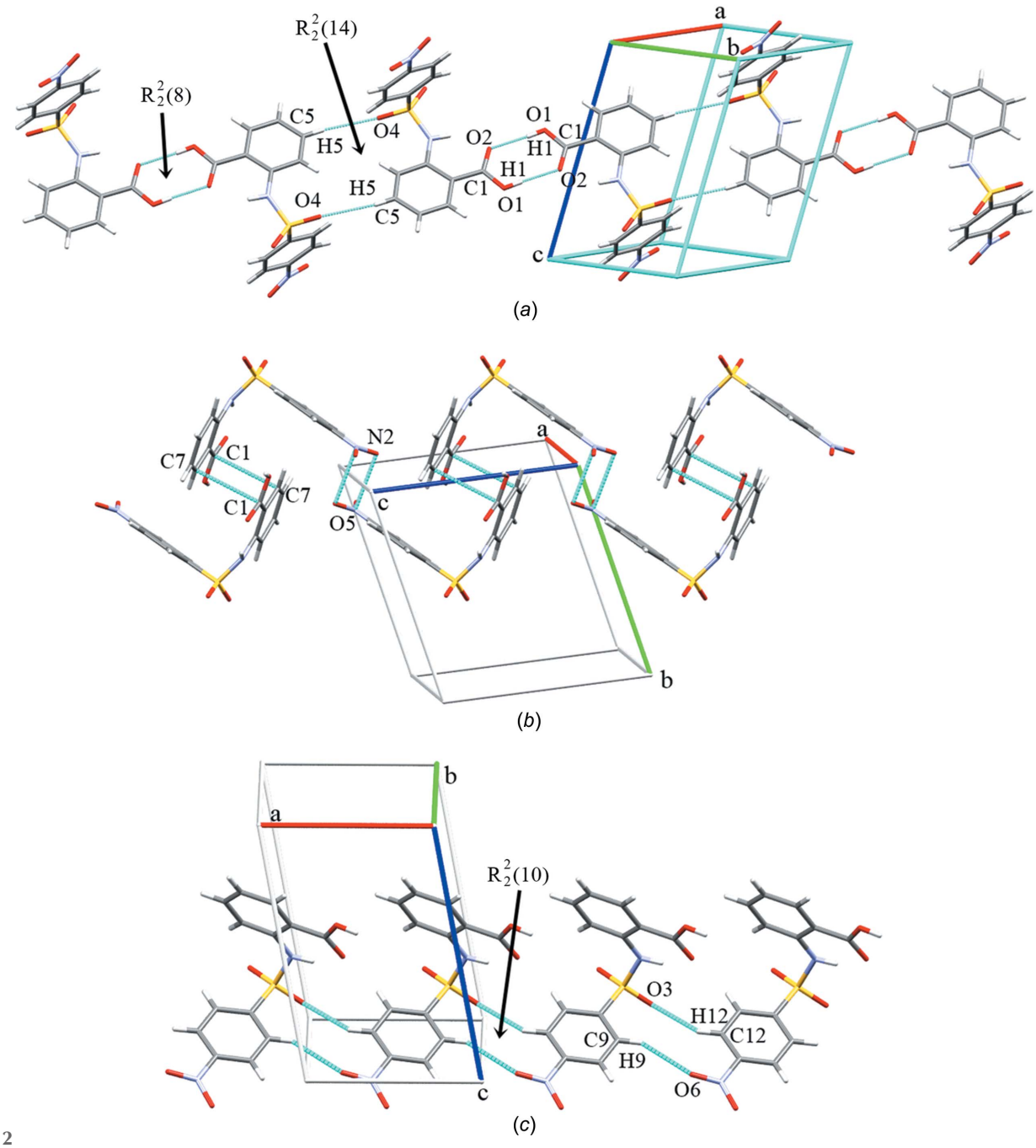

Figure 2
Intermolecular hydrogen bonds in the crystal structure of H*L*.

Table 3
Hydrogen-bond parameters (Å, °) for H*L* and Ag*L*.

D—H···*A*	*D*—H	H···*A*	*D*···*A*	*D*—H···*A*
H*L*				
N1—H1N···O2	0.85	1.94	2.655 (1)	141
C4—H4···O4	0.93	2.41	3.0729 (2)	128
O1—H1···O2^{i}	0.82	1.86	2.6766 (14)	174
C5—H5···O4^{ii}	0.93	2.60	3.5150 (17)	170
C9—H9···O6^{iii}	0.93	2.60	3.3511 (18)	138
C12—H12···O3^{iv}	0.93	2.62	3.3042 (17)	131
Ag*L*				
N1—H1N···O2	0.85	1.85	2.602 (3)	146
C4—H4···O4	0.93	2.41	3.062 (4)	127
C5—H5···O3^{v}	0.93	2.65	3.457 (4)	145
C10—H10···O4^{vi}	0.93	2.56	3.2063 (1)	157
C12—H12···O6^{vii}	0.93	2.49	3.369 (4)	157
C13—H13···O5^{viii}	0.93	2.70	3.424 (4)	136

Symmetry codes: (i) $-x+1, -y, -z+1$; (ii) $-x+1, -y+1, -z+1$; (iii) $x-1, y, z$; (iv) $x+1, y, z$; (v) x, y, z; (vi) $x, -y+\frac{3}{2}, z+\frac{1}{2}$; (vii) $-x, -y, -z$; (viii) $x, -y+\frac{1}{2}, z-\frac{1}{2}$.

C5—H5···O4^{ii} hydrogen bonds between neighbouring H*L* molecules form closed loops with graph-sets $R_2^2(8)$ and $R_2^2(14)$, respectively (Fig. 2*a* and Table 3). These two intermolecular hydrogen bonds form a one-dimensional (1D) layer in the [210] crystallographic direction. The propagation in the [101] crystallographic direction is associated with a lone-pair···π (lp···π) O5···N2 interaction (symmetry code: $-x+1, -y, -z+2$), with O5···N2 = 2.9172 (12) Å, and a π-stacking C1···C7 interaction (symmetry code: $-x, -y, -z+1$), with C1···C7 = 3.3380 (19) Å (Fig. 2*b*). The structure is also characterized by the presence of C9—H9···O6^{iii} and C12—H12···O3^{iv} hydrogen bonds, which form an $R_2^2(10)$ ring (Fig. 2*c*).

In Ag*L*, the Ag centre is coordinated to three O atoms (O1^{i}, O1^{ii} and O2) of three distinct monoanionic ligands (L^-), with Ag—O1^{i} varying from 2.290 (2) to 2.437 (2) Å (Table 2 and Fig. 3). The metal also shows a η^1 aromatic interaction with the phenyl C6 atom of a neighbouring molecule, with Ag···C6 = 2.551 (3) Å. This suggests a strong monohapto aromatic coordination to the Ag centre. Hence, the metal coordination sphere can be considered to contain Ag^{I} atoms with fourfold coordination. Moreover, analyzing the polymer structure, the Ag···Ag interaction, with Ag···Ag = 3.2926 (3) Å, may be considered a $d^{10}\cdots d^{10}$ noncovalent interaction (Sculfort & Braunstein, 2011), resulting in an OOOCAg···AgOOOC environment in the polymeric complex.

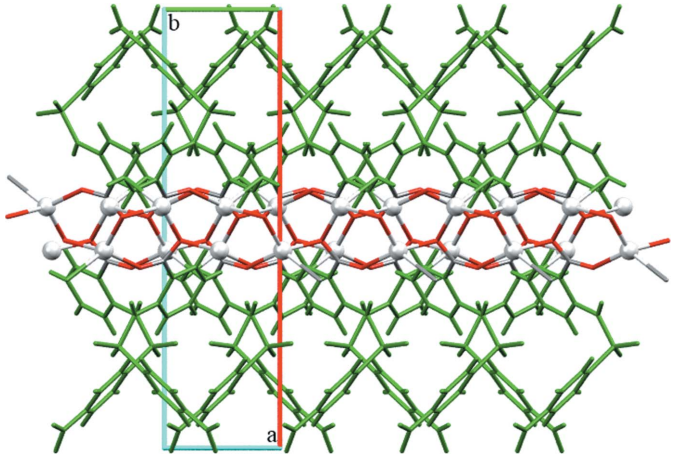

Figure 4
A capped sticks perspective view of the 1D coordination polymers in Ag*L* along the *c* direction. The Ag atoms are shown in ball-and-stick style. The intra- and intermolecular hydrogen bonds have been omitted for clarity.

The carboxylate group acts as a bridging group where the O atoms coordinate to two Ag^{I} ions in an anisobidentate mode (Fig. 3). Thus, the structure of the complex can be considered as a coordination polymer consisting of a 1D linear chain constructed by carboxylate bridging groups, running parallel to the *b* axis. Neighbouring polymeric chains are further bridged by Ag—C bonds, resulting in a 2D framework (Fig. 4). This shows the fundamental role exerted by the monohapto aromatic coordination in the packing and stability of the polymeric complex. The sulfonyl O atoms of Ag*L* act as acceptors in intermolecular hydrogen bonds from aromatic rings *A* (C5—H5···O3^{v}) and *B* (C10—H10···O4^{vi}), forming an $R_2^2(13)$ ring (Fig. 5). The phenyl–sulfonyl–phenyl unit results in an infinite chain parallel to the [010] direction. Interchain C12—H12···O6^{vii} and C13—H13···O5^{vii} hydrogen bonds extend the 2D polymer into a three-dimensional (3D) framework (Table 3).

3.3. Hirshfeld surface

On the Hirshfeld surfaces mapped over d_{norm} of H*L* (Fig. 6*a*), the short interatomic O···H/H···O interaction is observed as intense red spots near the carboxylic acid group. The light-red spots appearing near the phenyl H5, sulfonyl O4

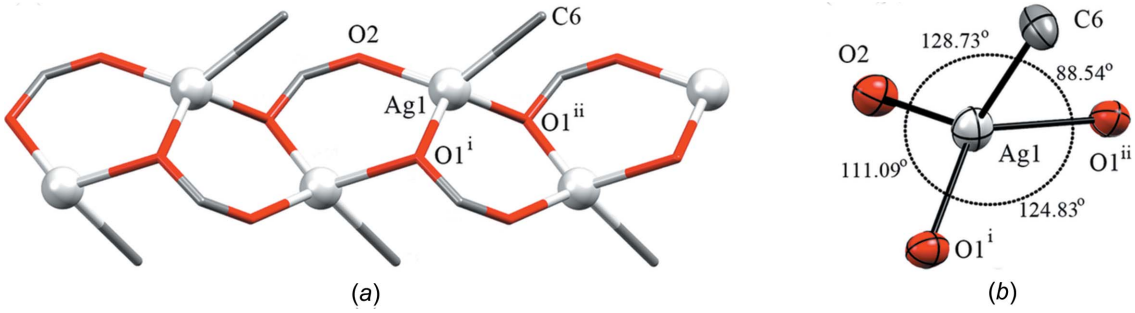

Figure 3
(*a*) A view in the *ab* plane of the propagation of Ag*L* along the [010] crystallographic direction. (*b*) The distorted tetrahedral geometry of the complex [O2—Ag1—O1^{ii} = 99.39 (8)°; symmetry code: (ii) $x, y+1, z$].

and nitro O6 atoms on the surface connect the molecules through interatomic O···H/H···O contacts (Fig. 6*b*). In addition, a faint-red spot near the nitro group shows the O···N/N···O interactions (green dashed) relative to the lp···π interaction in the crystal packing.

The Hirshfeld surface for Ag*L* shows light-red spots near the phenyl H12 and nitro O6 atoms that connect the molecules through interatomic O···H/H···O contacts (blue dashed lines in Fig. 7*a*). The Hirshfeld surface for Ag1 shows the bonds between the metal and the O atoms, as well as the monohapto interaction of the phenyl C6 atom and Ag1 that can be easily observed by the intense red spots (Fig. 7*b*). The red area in the 2D fingerprint plot of this surface (Fig. 7*c*) shows the high Ag···O/O···Ag contribution to the structure stability being associated with the three bonds between Ag^{I} and the O atoms of the carboxylate groups.

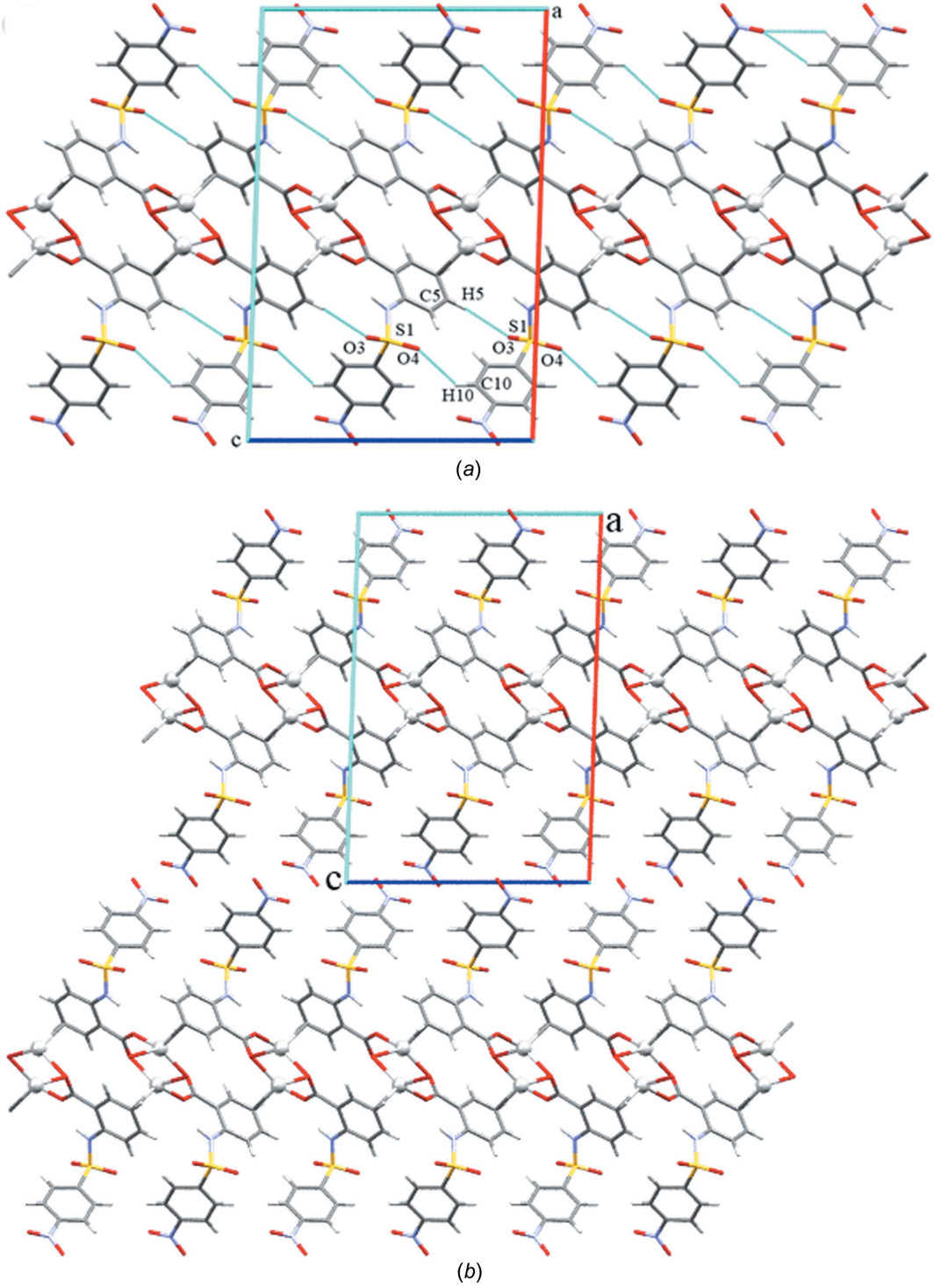

Figure 5
(*a*) Intermolecular hydrogen bonds and (*b*) the 2D network in the Ag*L* crystal structure. The Ag atoms are shown in ball-and-stick style.

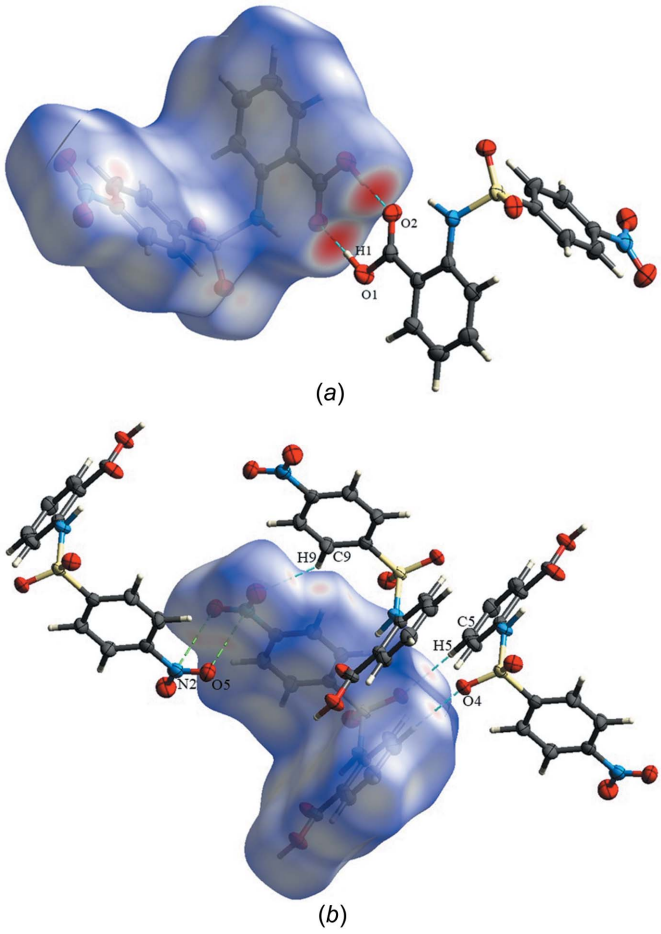

Figure 6
Hirshfeld surface for H*L* mapped over d_{norm} in the −0.600 to +1.200 a.u. range, highlighting (*a*) short interatomic O···H/H···O (blue dashed lines) and (*b*) N···O/O···N (green dashed lines) contacts.

The strong hydrogen bonds between the carboxylic acid group of two neighbouring molecules of the free ligand are observed as two spikes at $d_e + d_i \sim 1.7$ Å for H*L* in the 2D fingerprint plot (Fig. 8*b*). In Ag*L*, the O···H/H···O contacts present $d_e + d_i \sim 2.4$ Å related to coordination to Ag^I through the carboxylate site (Fig. 9*b*). Nevertheless, the percentage of O···H/H···O contacts is similar in H*L* and Ag*L*, *i.e.* 36.3 and 31.6%, respectively. The second most predominant contribution to the total Hirshfeld surface in H*L* and Ag*L* is the H···H interaction where the scattering points spread up at $d_e \simeq d_i <$ 1.2 Å (van der Waals radius of the H atom) (Fig. 8*c* and 9*c*), followed by the O···C/C···O interaction, which present similar pecentage in H*L* and Ag*L* (Fig. 8*d* and 9*d*).

In addition, from Hirshfeld surface analysis, it is noticed that the Ag···O/O···Ag region of the fingerprint plot for Ag*L* results in a spike with $d_e + d_i \sim 2.2$ Å, which is directly attributed to the Ag—O bonds in the polymer structure (Fig. 9*e*). The Ag···C/C···Ag interactions correspond to 4.4%, suggesting the relevance of the monohapto interaction in the crystal packing stability. Furthermore, the Ag···Ag interaction represent 0.5% of the interactions in the polymeric structure.

3.4. Human serum albumin (HSA) interaction analysis

Upon addition of increasing concentrations of the compounds under study, a decrease of the fluorescence maximum of HSA with a hypsochromic shift (*ca* 3 nm) is observed, indicating an increase of the hydrophobic microenvironment around the Trp-214 residue upon formation of the HSA–compound complex (Fig. 10). The values of the Stern–Volmer quenching constant (K_{SV}) and the bimolecular quenching rate constant (k_q) are listed in Table 4. The calculated values for the constants are higher than the quenching rate constant for diffusion-controlled processes (2.0×10^{10} l mol^{-1} s^{-1}) (Ware, 1962; Khan *et al.*, 2012). Hence, the fluorescence quenching of Trp-214 does not occur exclusively through a dynamic process, but the static mechanism might also be involved.

The values of the binding constant (K_b) for both compounds suggest a moderate interaction with the biomolecule,

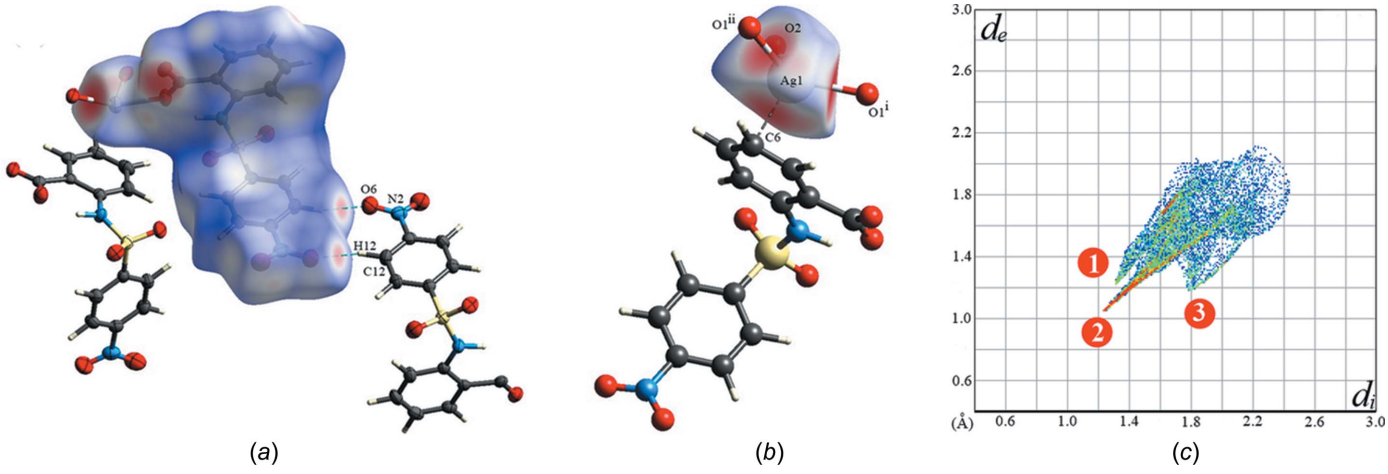

Figure 7
(*a*) Hirshfeld surface for Ag*L* mapped over d_{norm} highlighting short interatomic O···H/H···O contacts (blue dashed lines). (*b*) Hirshfeld surface for Ag1 mapped over d_{norm} with Ag···C/C···Ag as a black dashed line. (*c*) The 2D fingerprint plot of the surface of Ag1, emphasizing the regions for interactions Ag···C/C···Ag (**1**), Ag···O/O···Ag (**2**) and Ag···H/H···Ag (**3**).

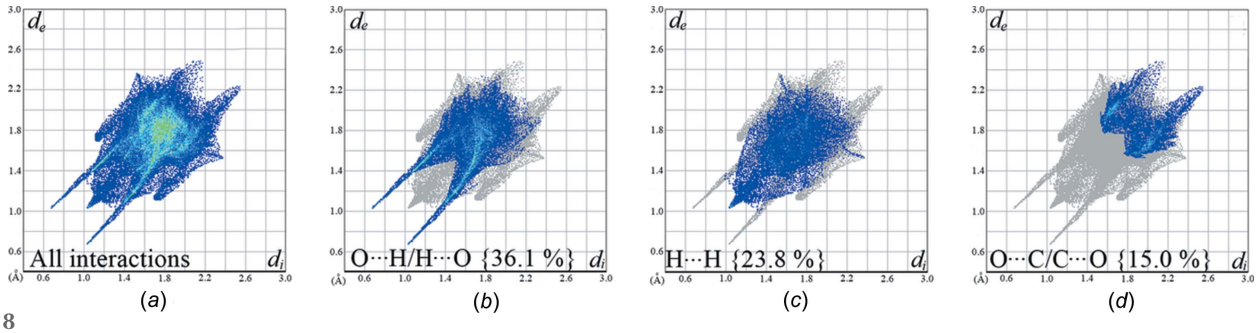

Figure 8
(*a*) The full 2D fingerprint plots of H*L* and (*b*)/(*c*)/(*d*) those delineated into O···H/H···O, H···H and O···C/C···O interactions, respectively, showing the percentage contributions to the Hirshfeld surface.

Table 4
Stern–Volmer quenching constant (K_{SV}), bimolecular quenching rate constant (k_q), binding constant (K_b), number of binding sites per protein (η) and free energy variation (ΔG) associated with the compound–HSA interaction in Tris-HCl Buffer (pH 7.2, λ_{exc} = 295 nm).

R^a is the correlation coefficient for the K_{SV} values and R^b is the correlation coefficient for the K_b values.

Compounds	K_{SV} (10^4 M^{-1})	k_q (10^{12} M^{-1} s^{-1})	R^a	K_b (10^4 M^{-1})	η	R^b	ΔG (kJ mol^{-1})
H*L*	5.15	5.15	0.9987	1.89	0.919	0.9973	−24.39
Ag*L*	4.50	4.50	0.9976	34.96	1.164	0.9917	−31.64

the Ag*L*–HSA interaction being 20-times stronger compared to H*L*–HSA. The correlation coefficients are larger than 0.99, indicating that the interactions are compatible with the binding model. The values of η were approximately equal to 1, suggesting a single binding site in HSA for the compounds. Moreover, the negative values of free energy changes suggest thermodynamic stability and spontaneous binding to HSA.

4. Conclusions

In the present work, a polymeric Ag*L* coordination framework based on 2-(4-nitrophenylsulfonamido)benzoic acid (H*L*) was prepared and characterized by NMR and FT–IR spectroscopies. The X-ray crystal structures of both compounds were determined by single-crystal X-ray diffraction. Structural analysis for H*L* shows a characteristic dimer formation *via* intermolecular O—H···O hydrogen bonding between the carboxylic acid groups of neighbouring molecules. The Ag*L* complex showed a polymeric structure with the Ag atom presenting an OOOAg···AgOOO environment and an Ag—C monohapto interaction. Hirshfeld surface analysis and 2D fingerprint plots indicate that the O···H/H···O interactions are more frequent in the crystal packing of both H*L* and Ag*L*, being essential to the stabilization of the

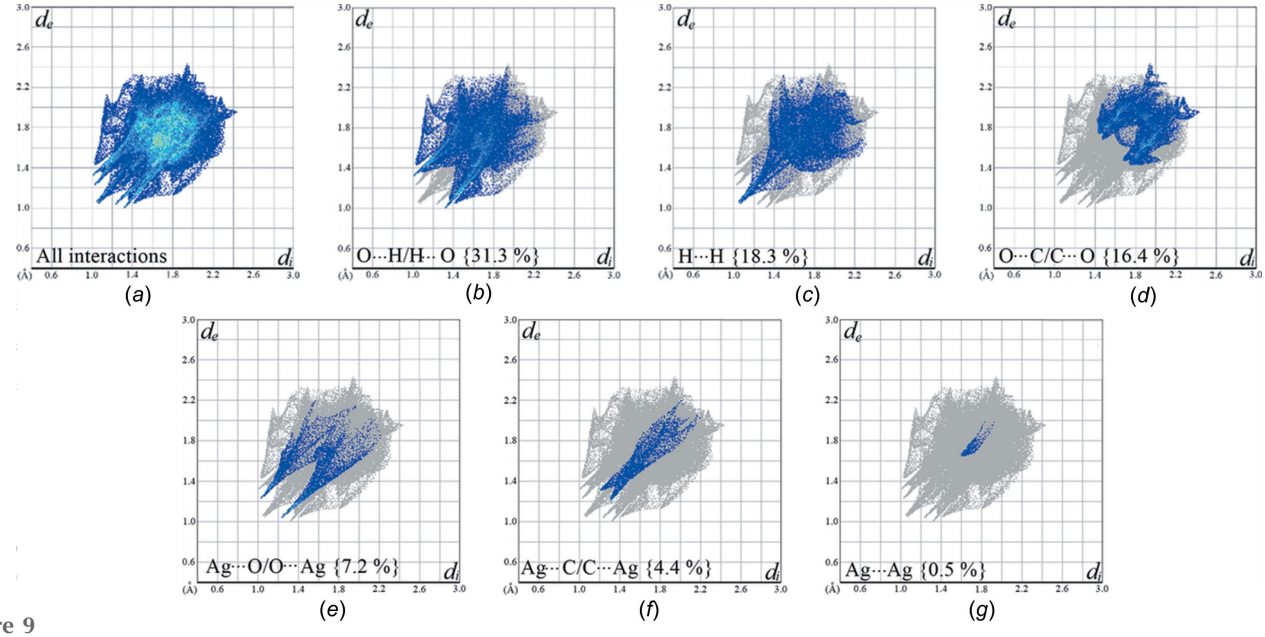

Figure 9
2D fingerprint plots of Ag*L*, showing (*a*) full and resolved into (*b*) O···H/H···O, (*c*) H···H, (*d*) O···C/C···O, (*e*) Ag···O/O···Ag, (*f*) Ag···C/C···Ag and (*g*) Ag···Ag interactions, showing the percentage contributions to the Hirshfeld surface.

crystal structure. Investigation of the interactions of H*L* and Ag*L* with HSA revealed that the compounds show a moderate affinity for HSA, the Ag*L*–HSA interaction being 20-times stronger compared to the H*L*–HSA interaction. The strong silver(I) complex interaction with the biomolecule suggests a potential application for this kind of compound for biological and the structure–activity studies.

Acknowledgements

The authors are grateful to Conselho Nacional de Desenvolvimento Científico e Tecnológico (CNPq) and Conselho de Aperfeiçoamento de Pessoal de Nível Superior (CAPES) Brazilian funding agencies for financial support.

References

Ascenzi, P., Fanali, G., Fasano, M., Pallottini, V. & Trezza, V. (2014). *J. Mol. Struct.* **1077**, 4–13.

Bomfim Filho, L. F. O., Parrilha, G. L., Ardisson, J. D., Beraldo, H., Teixeira, L. R. & Rodrigues, B. L. (2019). *J. Mol. Struct.* **1176**, 552–561.

Chen, L. Z., Pan, Q. J., Cao, X. X. & Wang, F. M. (2016). *CrystEngComm*, **18**, 1944–1952.

Deng, X. & Mani, N. S. (2006). *Green Chem.* **8**, 835–838.

Feng, S., Yang, H., Jiang, X., Wang, Y. & Zhu, M. (2015). *J. Mol. Struct.* **1081**, 1–5.

Guldiren, D. & Aydin, S. (2017). *Mater. Sci. Eng. C Mater. Biol. Appl.* **78**, 826–832.

Hussain, S. & Ferguson, C. (2006). *Emerg. Med. J.* **23**, 929–932.

Hussaini, S. Y., Haque, R. A. & Razali, M. R. (2019). *J. Organomet. Chem.* **882**, 96–111.

Igberase, E., Ofomaja, A. & Osifo, P. O. (2019). *Int. J. Biol. Macromol.* **123**, 664–676.

Khan, A. B., Khan, J. M., Ali, M. S., Khan, R. H. & Din, K. U. (2012). *Spectrochim. Acta A Mol. Biomol. Spectrosc.* **97**, 119–124.

Lakowicz, J. R. & Weber, G. (1973). *Biochemistry*, **12**, 4161–4170.

Li, M., Xiang, J., Yuan, L., Wu, S., Chen, S. & Sun, J. (2006). *Cryst. Growth Des.* **6**, 2036–2040.

Macrae, C. F., Bruno, I. J., Chisholm, J. A., Edgington, P. R., McCabe, P., Pidcock, E., Rodriguez-Monge, L., Taylor, R., van de Streek, J. & Wood, P. A. (2008). *J. Appl. Cryst.* **41**, 466–470.

Nakamoto, K. (2008). In *Infrared and Raman Spectra of Inorganic and Coordination Compounds*. Part A. *Theory and Applications in Inorganic Chemistry*, 6th ed. New York: Wiley.

Pan, M., Liao, W.-M., Yin, S.-Y., Sun, S.-S. & Su, C.-Y. (2018). *Chem. Rev.* **118**, 8889–8935.

Prior, A. M., Zhang, M., Blakeman, N., Datta, P., Pham, H., Chen, Q., Young, L. H., Weis, M. T. & Hua, D. H. (2014). *Bioorg. Med. Chem. Lett.* **24**, 1057–1061.

Rigaku OD (2018). *CrysAlis PRO*. Rigaku Oxford Diffraction Ltd, Yarnton, Oxfordshire, England.

Roca, S., Vikić-Topić, D., Plavec, J., Šket, P., Mihalić, Z., Matković-Čalogović, D. & Popović, Z. (2016). *Polyhedron*, **109**, 166–175.

Rosbottom, I., Toroz, D., Hammond, R. B. & Roberts, K. J. (2018). *CrystEngComm*, **20**, 7543–7555.

Santos, A. F., Ferreira, I. P., Takahashi, J. A., Rodrigues, G. L. S., Pinheiro, C. B., Teixeira, L. R., Rocha, W. R. & Beraldo, H. (2018). *New J. Chem.* **42**, 2125–2132.

Sculfort, S. & Braunstein, P. (2011). *Chem. Soc. Rev.* **40**, 2741–2760.

Shakuntala, K., Naveen, S., Lokanath, N. K., Suchetan, P. A. & Abdoh, M. (2017). *Acta Cryst.* C**73**, 833–844.

Sheldrick, G. M. (2008). *Acta Cryst.* A**64**, 112–122.

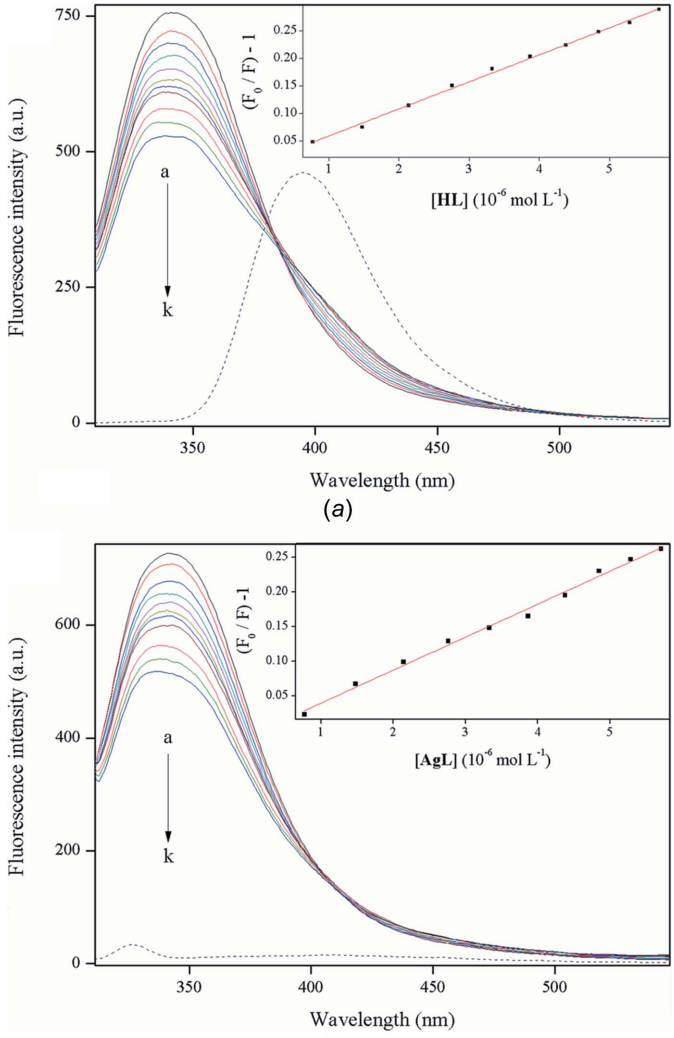

Figure 10
Fluorescence spectra of HSA in the absence (shown as **a**) and presence (**b**–**k**) of increasing concentrations of the compounds at 298 K for (*a*) H*L* and (*b*) Ag*L*. **a**–**k**: $r_{[compounds/HSA]}$ = 0.0–3.6, respectively. The black dotted lines are the fluorescence spectra (pH 7.2, λ_{exc} = 295 nm). Inset: Stern–Volmer plot of $(F_0/F) - 1$ *versus* [compound].

Sheldrick, G. M. (2015). *Acta Cryst.* C**71**, 3–8.

Spackman, M. A. & Jayatilaka, D. (2009). *CrystEngComm*, **11**, 19–32.

Spackman, M. A. & McKinnon, J. J. (2002). *CrystEngComm*, **4**, 378–392.

Tamayo, L. V., Santos, A. F., Ferreira, I. P., Santos, V. G., Lopes, M. T. P. & Beraldo, H. (2017). *Biometals*, **30**, 379–392.

Turner, M. J., McKinnon, J. J., Wolff, S. K., Grimwood, D. J., Spackman, P. R., Jayatilaka, D. & Spackman, M. A. (2017). *CrystalExplorer*. Version 17. University of Western Australia. http://crystalexplorer.scb.uwa.edu.au/.

Ware, W. R. (1962). *J. Phys. Chem.* **66**, 455–458.

Wu, X. Y., Qi, H. X., Ning, J. J., Wang, J. F., Ren, Z. G. & Lang, J. P. (2015). *Appl. Catal. Environ.* **168–169**, 98–104.

Yang, Y. Y., Zhou, L. X., Zheng, Y. Q. & Zhu, H. L. (2017). *Polyhedron*, **134**, 345–355.

Yilmaz, V. T., Icsel, C., Batur, J., Aydinlik, S., Cengiz, M. & Buyukgungor, O. (2017). *Dalton Trans.* **46**, 8110–8124.

supporting information

Acta Cryst. (2019). C**75**, 1011-1020 [https://doi.org/10.1107/S2053229619008593]

Synthesis, crystal structure and studies on the interaction with albumin of a new silver(I) complex based on 2-(4-nitrobenzenesulfonamido)benzoic acid

Lucius Flavius Ourives Bomfim Filho, Cleidivania Rocha, Bernardo Lages Rodrigues, Heloisa Beraldo and Leticia Regina Teixeira

Computing details

For both structures, data collection: *CrysAlis PRO* (Rigaku OD, 2018); cell refinement: *CrysAlis PRO* (Rigaku OD, 2018); data reduction: *CrysAlis PRO* (Rigaku OD, 2018); program(s) used to solve structure: *SHELXS97* (Sheldrick, 2008); program(s) used to refine structure: *SHELXL2018* (Sheldrick, 2015); molecular graphics: *Mercury* (Macrae *et al.*, 2008); software used to prepare material for publication: *SHELXL2018* (Sheldrick, 2015).

2-(4-Nitrobenzenesulfonamido)benzoic acid (HL)

Crystal data

$C_{13}H_{10}N_2O_6S$
$M_r = 322.29$
Triclinic, $P\overline{1}$
Hall symbol: -P 1
$a = 6.9140$ (3) Å
$b = 10.0641$ (5) Å
$c = 10.1532$ (5) Å
$\alpha = 102.153$ (4)°
$\beta = 100.951$ (4)°
$\gamma = 99.745$ (4)°
$V = 661.77$ (6) Å^3
$Z = 2$
$F(000) = 332$
$D_x = 1.617$ Mg m^{-3}
Mo $K\alpha$ radiation, $\lambda = 0.71073$ Å
Cell parameters from 5557 reflections
$\theta = 3.1$–32.6°
$\mu = 0.28$ mm^{-1}
$T = 301$ K
Prism, colourless
0.68 × 0.35 × 0.14 mm

Data collection

Rigaku Xcalibur, Atlas, Gemini ultra diffractometer
Graphite monochromator
Detector resolution: 10.4186 pixels mm^{-1}
ω scans
Absorption correction: multi-scan (CrysAlis PRO; Rigaku OD, 2018)
$T_{min} = 0.901$, $T_{max} = 1.000$
13718 measured reflections
4515 independent reflections
3841 reflections with $I > 2\sigma(I)$
$R_{int} = 0.043$
$\theta_{max} = 32.8°$, $\theta_{min} = 2.6°$
$h = -10 \rightarrow 10$
$k = -14 \rightarrow 14$
$l = -15 \rightarrow 14$

Refinement

Refinement on F^2
Least-squares matrix: full
$R[F^2 > 2\sigma(F^2)] = 0.041$
$wR(F^2) = 0.116$
$S = 1.06$
4515 reflections
200 parameters
0 restraints
Hydrogen site location: mixed
H-atom parameters constrained
$w = 1/[\sigma^2(F_o^2) + (0.0534P)^2 + 0.1382P]$ where $P = (F_o^2 + 2F_c^2)/3$

$(\Delta/\sigma)_{max} < 0.001$
$\Delta\rho_{max} = 0.33$ e Å^{-3}
$\Delta\rho_{min} = -0.37$ e Å^{-3}

Special details

Geometry. All esds (except the esd in the dihedral angle between two l.s. planes) are estimated using the full covariance matrix. The cell esds are taken into account individually in the estimation of esds in distances, angles and torsion angles; correlations between esds in cell parameters are only used when they are defined by crystal symmetry. An approximate (isotropic) treatment of cell esds is used for estimating esds involving l.s. planes.

Refinement. Single-crystal X-ray diffraction measurements were performed on an Agilent–Gemini diffractometer equipped with a CCD area detector using MoK? (0.71073 Å) radiation. The *CrysAlisPro* software package (Rigaku, 2015) was used for data collection and reduction (Oxford Diffraction Ltda, version 171.38.41). The structures were solved by direct methods using SHELXS-97 and refined by full-matrix least squares on F^2 using SHELXL-2018 (Sheldrick, 2015). All non-hydrogen atoms were refined using anisotropic displacement parameters.

Fractional atomic coordinates and isotropic or equivalent isotropic displacement parameters (Å²)

	x	*y*	*z*	U_{iso}*/U_{eq}
S1	0.12454 (4)	0.47628 (3)	0.74105 (3)	0.02885 (9)
O1	−0.33898 (16)	−0.03940 (10)	0.38167 (11)	0.0433 (2)
H1	−0.443606	−0.066604	0.404167	0.065*
O2	−0.32527 (14)	0.14767 (10)	0.54881 (12)	0.0406 (2)
O3	−0.01498 (16)	0.51483 (10)	0.82160 (11)	0.0403 (2)
O4	0.25416 (15)	0.58008 (10)	0.70247 (11)	0.0393 (2)
O5	0.58057 (18)	0.11306 (11)	1.12775 (11)	0.0458 (3)
O6	0.79937 (17)	0.14961 (13)	1.00541 (14)	0.0546 (3)
N1	−0.01504 (15)	0.36229 (11)	0.60268 (11)	0.0308 (2)
H1N	−0.129422	0.323849	0.611424	0.037*
N2	0.64156 (17)	0.16245 (12)	1.03919 (12)	0.0358 (2)
C1	−0.25207 (18)	0.08679 (13)	0.45781 (13)	0.0307 (2)
C2	−0.06143 (17)	0.14679 (12)	0.42646 (12)	0.0276 (2)
C3	0.05425 (17)	0.28066 (12)	0.49812 (12)	0.0265 (2)
C4	0.2329 (2)	0.33032 (15)	0.46234 (14)	0.0361 (3)
H4	0.30801	0.419659	0.507179	0.043*
C5	0.2993 (2)	0.24796 (17)	0.36091 (16)	0.0418 (3)
H5	0.420223	0.281618	0.33951	0.05*
C6	0.1880 (2)	0.11621 (16)	0.29097 (15)	0.0414 (3)
H6	0.233994	0.060917	0.223264	0.05*
C7	0.0083 (2)	0.06735 (14)	0.32238 (14)	0.0364 (3)
H7	−0.068407	−0.020376	0.273293	0.044*
C8	0.28090 (17)	0.38494 (12)	0.83002 (12)	0.0280 (2)
C9	0.2009 (2)	0.30539 (16)	0.91162 (16)	0.0380 (3)
H9	0.068394	0.301506	0.919686	0.046*
C10	0.3196 (2)	0.23221 (15)	0.98058 (15)	0.0373 (3)
H10	0.268501	0.178123	1.035203	0.045*
C11	0.51523 (19)	0.24128 (12)	0.96650 (13)	0.0300 (2)
C12	0.5970 (2)	0.32060 (15)	0.88735 (15)	0.0370 (3)
H12	0.72984	0.324516	0.880113	0.044*
C13	0.47850 (19)	0.39464 (15)	0.81850 (14)	0.0349 (3)
H13	0.53117	0.449933	0.765428	0.042*

Atomic displacement parameters (Å²)

	U^{11}	U^{22}	U^{33}	U^{12}	U^{13}	U^{23}
S1	0.02764 (15)	0.02435 (15)	0.03087 (16)	0.00152 (11)	0.00438 (11)	0.00453 (11)
O1	0.0386 (5)	0.0351 (5)	0.0449 (6)	−0.0104 (4)	0.0123 (4)	−0.0017 (4)
O2	0.0288 (4)	0.0346 (5)	0.0517 (6)	−0.0038 (4)	0.0147 (4)	0.0000 (4)
O3	0.0398 (5)	0.0385 (5)	0.0421 (5)	0.0128 (4)	0.0122 (4)	0.0032 (4)
O4	0.0375 (5)	0.0283 (4)	0.0465 (6)	−0.0046 (4)	0.0031 (4)	0.0126 (4)
O5	0.0538 (6)	0.0428 (6)	0.0410 (6)	0.0088 (5)	0.0051 (5)	0.0176 (5)
O6	0.0403 (6)	0.0572 (7)	0.0746 (9)	0.0202 (5)	0.0156 (6)	0.0252 (6)
N1	0.0230 (4)	0.0315 (5)	0.0319 (5)	−0.0014 (4)	0.0053 (4)	0.0022 (4)
N2	0.0355 (6)	0.0292 (5)	0.0378 (6)	0.0047 (4)	0.0019 (4)	0.0056 (4)
C1	0.0255 (5)	0.0294 (6)	0.0331 (6)	−0.0002 (4)	0.0031 (4)	0.0071 (5)
C2	0.0251 (5)	0.0295 (5)	0.0266 (5)	0.0017 (4)	0.0043 (4)	0.0081 (4)
C3	0.0245 (5)	0.0288 (5)	0.0248 (5)	0.0022 (4)	0.0032 (4)	0.0087 (4)
C4	0.0309 (6)	0.0377 (7)	0.0360 (6)	−0.0037 (5)	0.0097 (5)	0.0086 (5)
C5	0.0376 (7)	0.0519 (8)	0.0392 (7)	0.0040 (6)	0.0172 (6)	0.0160 (6)
C6	0.0457 (8)	0.0464 (8)	0.0355 (7)	0.0098 (6)	0.0192 (6)	0.0092 (6)
C7	0.0414 (7)	0.0345 (6)	0.0303 (6)	0.0035 (5)	0.0095 (5)	0.0041 (5)
C8	0.0261 (5)	0.0274 (5)	0.0277 (5)	0.0018 (4)	0.0051 (4)	0.0055 (4)
C9	0.0279 (6)	0.0468 (8)	0.0460 (8)	0.0078 (5)	0.0147 (5)	0.0207 (6)
C10	0.0345 (6)	0.0420 (7)	0.0413 (7)	0.0059 (5)	0.0139 (5)	0.0202 (6)
C11	0.0303 (6)	0.0269 (5)	0.0291 (5)	0.0035 (4)	0.0036 (4)	0.0042 (4)
C12	0.0266 (6)	0.0461 (7)	0.0417 (7)	0.0067 (5)	0.0114 (5)	0.0158 (6)
C13	0.0295 (6)	0.0415 (7)	0.0364 (6)	0.0036 (5)	0.0109 (5)	0.0159 (5)

Geometric parameters (Å, º)

S1—O4	1.4271 (10)	C4—H4	0.93
S1—O3	1.4293 (10)	C5—C6	1.380 (2)
S1—N1	1.6287 (11)	C5—H5	0.93
S1—C8	1.7733 (12)	C6—C7	1.378 (2)
O1—C1	1.3128 (15)	C6—H6	0.93
O1—H1	0.82	C7—H7	0.93
O2—C1	1.2368 (16)	C8—C13	1.3821 (17)
O5—N2	1.2226 (16)	C8—C9	1.3919 (17)
O6—N2	1.2232 (16)	C9—C10	1.3818 (19)
N1—C3	1.4109 (16)	C9—H9	0.93
N1—H1N	0.8488	C10—C11	1.3771 (18)
N2—C11	1.4742 (16)	C10—H10	0.93
C1—C2	1.4745 (17)	C11—C12	1.3758 (18)
C2—C7	1.3988 (18)	C12—C13	1.3869 (19)
C2—C3	1.4091 (16)	C12—H12	0.93
C3—C4	1.3950 (17)	C13—H13	0.93
C4—C5	1.381 (2)		
O4—S1—O3	120.22 (6)	C6—C5—H5	119.7
O4—S1—N1	109.78 (6)	C4—C5—H5	119.7

O3—S1—N1	104.49 (6)	C7—C6—C5	119.39 (13)
O4—S1—C8	107.12 (6)	C7—C6—H6	120.3
O3—S1—C8	108.39 (6)	C5—C6—H6	120.3
N1—S1—C8	106.03 (6)	C6—C7—C2	121.45 (13)
C1—O1—H1	109.5	C6—C7—H7	119.3
C3—N1—S1	126.42 (8)	C2—C7—H7	119.3
C3—N1—H1N	113.2	C13—C8—C9	121.35 (12)
S1—N1—H1N	114.7	C13—C8—S1	119.98 (10)
O5—N2—O6	124.50 (12)	C9—C8—S1	118.67 (9)
O5—N2—C11	117.92 (12)	C10—C9—C8	119.56 (12)
O6—N2—C11	117.58 (12)	C10—C9—H9	120.2
O2—C1—O1	121.85 (11)	C8—C9—H9	120.2
O2—C1—C2	123.80 (11)	C11—C10—C9	118.42 (12)
O1—C1—C2	114.34 (11)	C11—C10—H10	120.8
C7—C2—C3	118.68 (11)	C9—C10—H10	120.8
C7—C2—C1	118.77 (11)	C12—C11—C10	122.67 (12)
C3—C2—C1	122.55 (11)	C12—C11—N2	118.86 (11)
C4—C3—C2	119.19 (11)	C10—C11—N2	118.47 (12)
C4—C3—N1	121.53 (11)	C11—C12—C13	119.04 (12)
C2—C3—N1	119.27 (10)	C11—C12—H12	120.5
C5—C4—C3	120.56 (13)	C13—C12—H12	120.5
C5—C4—H4	119.7	C8—C13—C12	118.95 (12)
C3—C4—H4	119.7	C8—C13—H13	120.5
C6—C5—C4	120.67 (13)	C12—C13—H13	120.5

O4—S1—N1—C3	57.75 (12)	O4—S1—C8—C13	−17.03 (12)
O3—S1—N1—C3	−172.05 (10)	O3—S1—C8—C13	−148.14 (11)
C8—S1—N1—C3	−57.63 (12)	N1—S1—C8—C13	100.16 (11)
O2—C1—C2—C7	179.10 (13)	O4—S1—C8—C9	162.39 (11)
O1—C1—C2—C7	−0.05 (17)	O3—S1—C8—C9	31.28 (12)
O2—C1—C2—C3	−0.3 (2)	N1—S1—C8—C9	−80.42 (12)
O1—C1—C2—C3	−179.48 (11)	C13—C8—C9—C10	−1.3 (2)
C7—C2—C3—C4	0.65 (18)	S1—C8—C9—C10	179.30 (11)
C1—C2—C3—C4	−179.91 (11)	C8—C9—C10—C11	0.3 (2)
C7—C2—C3—N1	179.55 (11)	C9—C10—C11—C12	0.3 (2)
C1—C2—C3—N1	−1.01 (17)	C9—C10—C11—N2	−179.56 (12)
S1—N1—C3—C4	−32.39 (17)	O5—N2—C11—C12	167.21 (13)
S1—N1—C3—C2	148.74 (10)	O6—N2—C11—C12	−13.63 (18)
C2—C3—C4—C5	−2.0 (2)	O5—N2—C11—C10	−12.89 (18)
N1—C3—C4—C5	179.15 (12)	O6—N2—C11—C10	166.27 (13)
C3—C4—C5—C6	1.4 (2)	C10—C11—C12—C13	−0.1 (2)
C4—C5—C6—C7	0.5 (2)	N2—C11—C12—C13	179.83 (12)
C5—C6—C7—C2	−1.8 (2)	C9—C8—C13—C12	1.6 (2)
C3—C2—C7—C6	1.3 (2)	S1—C8—C13—C12	−179.04 (11)
C1—C2—C7—C6	−178.20 (13)	C11—C12—C13—C8	−0.9 (2)

Hydrogen-bond geometry (Å, º)

D—H···*A*	*D*—H	H···*A*	*D*···*A*	*D*—H···*A*
O1—H1···O2^{i}	0.82	1.86	2.6766 (14)	174
C5—H5···O4^{ii}	0.93	2.6	3.5150 (17)	170
C9—H9···O6^{iii}	0.93	2.6	3.3511 (18)	138

Symmetry codes: (i) −*x*−1, −*y*, −*z*+1; (ii) −*x*+1, −*y*+1, −*z*+1; (iii) *x*−1, *y*, *z*.

(AgL)

Crystal data

[Ag($C_{13}H_9N_2O_6S$)]
M_r = 429.15
Monoclinic, $P2_1/c$
Hall symbol: -P 2ybc
a = 19.9216 (7) Å
b = 5.2391 (2) Å
c = 13.0860 (4) Å
β = 91.864 (3)°
V = 1365.08 (8) Å^3
Z = 4
F(000) = 848
D_x = 2.088 Mg m^{-3}
Mo *Kα* radiation, *λ* = 0.71073 Å
Cell parameters from 8451 reflections
θ = 3.1–26.7°
μ = 1.67 mm^{-1}
T = 293 K
Irregular, colourless
0.21 × 0.18 × 0.17 mm

Data collection

Rigaku Xcalibur, Atlas, Gemini ultra diffractometer
Graphite monochromator
Detector resolution: 10.4186 pixels mm^{-1}
ω scans
Absorption correction: multi-scan (CrysAlis PRO; Rigaku OD, 2018)
T_{min} = 0.601, T_{max} = 1.000
22926 measured reflections
3553 independent reflections
2723 reflections with $I > 2\sigma(I)$
R_{int} = 0.046
θ_{max} = 29.5°, θ_{min} = 3.1°
h = −27→26
k = −7→7
l = −18→16

Refinement

Refinement on F^2
Least-squares matrix: full
$R[F^2 > 2\sigma(F^2)]$ = 0.037
$wR(F^2)$ = 0.082
S = 1.07
3553 reflections
208 parameters
0 restraints
Hydrogen site location: mixed
H-atom parameters constrained
$w = 1/[\sigma^2(F_o^2) + (0.0311P)^2 + 1.0461P]$ where $P = (F_o^2 + 2F_c^2)/3$
$(\Delta/\sigma)_{max}$ = 0.001
$\Delta\rho_{max}$ = 0.82 e Å^{-3}
$\Delta\rho_{min}$ = −0.78 e Å^{-3}

Special details

Geometry. All esds (except the esd in the dihedral angle between two l.s. planes) are estimated using the full covariance matrix. The cell esds are taken into account individually in the estimation of esds in distances, angles and torsion angles; correlations between esds in cell parameters are only used when they are defined by crystal symmetry. An approximate (isotropic) treatment of cell esds is used for estimating esds involving l.s. planes.

Refinement. Single-crystal X-ray diffraction measurements were performed on an Agilent–Gemini diffractometer equipped with a CCD area detector using MoK? (0.71073 Å) radiation. The *CrysAlisPro* software package (Rigaku, 2015) was used for data collection and reduction (Oxford Diffraction Ltda, version 171.38.41). The structures were solved by direct methods using SHELXS-97 and refined by full-matrix least squares on F^2 using SHELXL-2018 (Sheldrick, 2015). All non-hydrogen atoms were refined using anisotropic displacement parameters.

Fractional atomic coordinates and isotropic or equivalent isotropic displacement parameters (Å²)

	x	*y*	*z*	U_{iso}*/U_{eq}
Ag1	0.45005 (2)	1.02405 (5)	0.25327 (2)	0.04349 (10)
S1	0.23113 (4)	0.89424 (14)	0.01834 (6)	0.03421 (18)
O1	0.47283 (10)	0.3610 (4)	0.13073 (16)	0.0406 (5)
O2	0.41107 (11)	0.7127 (4)	0.14202 (16)	0.0445 (5)
O3	0.23823 (11)	1.0962 (4)	0.09090 (18)	0.0451 (6)
O4	0.21229 (12)	0.9467 (4)	−0.08584 (18)	0.0482 (6)
O5	0.05200 (13)	0.0407 (5)	0.2615 (2)	0.0599 (7)
O6	−0.00680 (14)	0.0579 (5)	0.1205 (2)	0.0663 (8)
N1	0.30383 (12)	0.7539 (5)	0.02430 (19)	0.0351 (6)
H1N	0.33012	0.786538	0.075391	0.042*
N2	0.04063 (14)	0.1248 (5)	0.1763 (2)	0.0448 (7)
C1	0.42645 (14)	0.5073 (5)	0.0991 (2)	0.0315 (6)
C2	0.38807 (13)	0.4301 (5)	0.0032 (2)	0.0282 (6)
C3	0.32950 (14)	0.5556 (5)	−0.0338 (2)	0.0299 (6)
C4	0.29988 (17)	0.4801 (6)	−0.1271 (2)	0.0420 (8)
H4	0.261568	0.563509	−0.152159	0.05*
C5	0.32676 (17)	1.2170 (6)	0.3173 (2)	0.0450 (8)
H5	0.306998	1.262994	0.254646	0.054*
C6	0.38302 (17)	1.3464 (6)	0.3546 (2)	0.0420 (8)
H6	0.400465	1.482049	0.318074	0.05*
C7	0.41304 (15)	1.2716 (5)	0.4467 (2)	0.0358 (7)
H7	0.450893	1.358491	0.471398	0.043*
C8	0.17263 (14)	0.6715 (5)	0.0643 (2)	0.0309 (6)
C9	0.17305 (15)	0.6189 (6)	0.1683 (2)	0.0376 (7)
H9	0.202846	0.703349	0.212837	0.045*
C10	0.12919 (16)	0.4414 (6)	0.2050 (2)	0.0385 (7)
H10	0.128829	0.403094	0.274379	0.046*
C11	0.08587 (14)	0.3220 (6)	0.1366 (2)	0.0347 (7)
C12	0.08370 (15)	0.3743 (6)	0.0338 (2)	0.0409 (7)
H12	0.053164	0.291552	−0.01005	0.049*
C13	0.12790 (16)	0.5524 (6)	−0.0029 (2)	0.0397 (7)
H13	0.127533	0.591882	−0.072238	0.048*

Atomic displacement parameters (Å²)

	U^{11}	U^{22}	U^{33}	U^{12}	U^{13}	U^{23}
Ag1	0.04819 (17)	0.04274 (16)	0.03908 (16)	−0.00480 (11)	−0.00562 (11)	−0.00134 (11)
S1	0.0330 (4)	0.0303 (4)	0.0392 (4)	0.0023 (3)	−0.0008 (3)	0.0045 (3)
O1	0.0330 (11)	0.0440 (12)	0.0444 (13)	−0.0003 (9)	−0.0045 (9)	0.0083 (10)
O2	0.0459 (13)	0.0461 (13)	0.0406 (13)	0.0017 (10)	−0.0098 (10)	−0.0123 (11)
O3	0.0450 (13)	0.0298 (11)	0.0605 (15)	0.0014 (9)	0.0011 (11)	−0.0065 (11)
O4	0.0484 (14)	0.0511 (14)	0.0449 (14)	0.0014 (11)	−0.0049 (11)	0.0193 (11)
O5	0.0645 (18)	0.0561 (16)	0.0593 (18)	−0.0083 (12)	0.0054 (14)	0.0165 (13)
O6	0.0653 (18)	0.0734 (18)	0.0604 (17)	−0.0333 (15)	0.0068 (14)	−0.0132 (14)
N1	0.0314 (13)	0.0384 (14)	0.0350 (14)	0.0029 (10)	−0.0049 (10)	−0.0071 (11)

N2	0.0419 (16)	0.0411 (15)	0.0520 (18)	−0.0050 (12)	0.0104 (13)	−0.0079 (14)
C1	0.0263 (14)	0.0366 (16)	0.0317 (15)	−0.0057 (12)	0.0044 (11)	0.0058 (13)
C2	0.0276 (14)	0.0300 (14)	0.0271 (14)	−0.0056 (11)	0.0050 (11)	0.0025 (11)
C3	0.0319 (15)	0.0309 (14)	0.0272 (14)	−0.0068 (11)	0.0037 (11)	0.0021 (11)
C4	0.0436 (18)	0.050 (2)	0.0323 (16)	−0.0041 (14)	−0.0059 (13)	−0.0014 (14)
C5	0.057 (2)	0.050 (2)	0.0287 (16)	0.0137 (16)	0.0040 (14)	0.0086 (14)
C6	0.052 (2)	0.0372 (17)	0.0374 (18)	0.0081 (14)	0.0151 (15)	0.0062 (14)
C7	0.0376 (16)	0.0327 (15)	0.0378 (17)	0.0021 (12)	0.0104 (13)	−0.0008 (13)
C8	0.0303 (15)	0.0302 (14)	0.0320 (15)	0.0046 (11)	−0.0012 (11)	0.0001 (12)
C9	0.0390 (17)	0.0404 (17)	0.0334 (16)	−0.0044 (13)	−0.0010 (13)	−0.0055 (13)
C10	0.0435 (18)	0.0437 (18)	0.0284 (16)	−0.0035 (14)	0.0040 (13)	−0.0014 (13)
C11	0.0320 (15)	0.0344 (16)	0.0380 (17)	0.0003 (12)	0.0049 (12)	−0.0034 (13)
C12	0.0373 (17)	0.0449 (18)	0.0401 (18)	−0.0048 (14)	−0.0063 (13)	−0.0047 (15)
C13	0.0397 (17)	0.0492 (18)	0.0299 (16)	−0.0012 (14)	−0.0040 (13)	0.0024 (14)

Geometric parameters (Å, º)

Ag1—O1^{i}	2.290 (2)	C2—C7^{iv}	1.391 (4)
Ag1—O2	2.304 (2)	C2—C3	1.411 (4)
Ag1—O1^{ii}	2.437 (2)	C3—C4	1.396 (4)
Ag1—C6	2.551 (3)	C4—C5^{iv}	1.381 (5)
Ag1—Ag1^{i}	3.2926 (3)	C4—H4	0.93
Ag1—Ag1^{iii}	3.2926 (3)	C5—C6	1.385 (5)
S1—O3	1.426 (2)	C5—H5	0.93
S1—O3	1.426 (2)	C6—C7	1.385 (4)
S1—O4	1.429 (2)	C6—H6	0.93
S1—N1	1.624 (2)	C7—H7	0.93
S1—C8	1.768 (3)	C8—C13	1.380 (4)
O1—C1	1.260 (3)	C8—C9	1.389 (4)
O2—C1	1.256 (3)	C9—C10	1.373 (4)
O3—O3	0.000 (4)	C9—H9	0.93
O5—N2	1.214 (4)	C10—C11	1.373 (4)
O6—N2	1.226 (4)	C10—H10	0.93
N1—C3	1.394 (4)	C11—C12	1.372 (4)
N1—H1N	0.8531	C12—C13	1.381 (4)
N2—C11	1.476 (4)	C12—H12	0.93
C1—C2	1.504 (4)	C13—H13	0.93
O1^{i}—Ag1—O2	111.09 (8)	C7^{iv}—C2—C3	118.5 (3)
O1^{i}—Ag1—O1^{ii}	124.83 (6)	C7^{iv}—C2—C1	117.9 (3)
O2—Ag1—O1^{ii}	99.39 (8)	C3—C2—C1	123.6 (3)
O1^{i}—Ag1—C6	104.70 (9)	N1—C3—C4	122.4 (3)
O2—Ag1—C6	128.73 (10)	N1—C3—C2	118.3 (2)
O1^{ii}—Ag1—C6	88.52 (9)	C4—C3—C2	119.3 (3)
O1^{i}—Ag1—Ag1^{i}	85.46 (6)	C5^{iv}—C4—C3	120.8 (3)
O2—Ag1—Ag1^{i}	137.59 (6)	C5^{iv}—C4—H4	119.6
O1^{ii}—Ag1—Ag1^{i}	44.04 (5)	C3—C4—H4	119.6
C6—Ag1—Ag1^{i}	79.27 (8)	C4^{vi}—C5—C6	120.3 (3)

O1^{i}—Ag1—Ag1^{iii}	47.72 (5)	C4^{vi}—C5—H5	119.9
O2—Ag1—Ag1^{iii}	67.17 (5)	C6—C5—H5	119.9
O1^{ii}—Ag1—Ag1^{iii}	115.69 (5)	C7—C6—C5	119.3 (3)
C6—Ag1—Ag1^{iii}	150.14 (7)	C7—C6—Ag1	92.67 (19)
Ag1^{i}—Ag1—Ag1^{iii}	105.420 (14)	C5—C6—Ag1	85.7 (2)
O3—S1—O3	0.00 (18)	C7—C6—H6	120.3
O3—S1—O4	120.67 (14)	C5—C6—H6	120.3
O3—S1—O4	120.67 (14)	Ag1—C6—H6	91.6
O3—S1—N1	103.59 (13)	C6—C7—C2^{vi}	121.7 (3)
O3—S1—N1	103.59 (13)	C6—C7—H7	119.1
O4—S1—N1	109.82 (14)	C2^{vi}—C7—H7	119.1
O3—S1—C8	108.40 (14)	C13—C8—C9	121.2 (3)
O3—S1—C8	108.40 (14)	C13—C8—S1	120.0 (2)
O4—S1—C8	107.19 (14)	C9—C8—S1	118.7 (2)
N1—S1—C8	106.35 (13)	C10—C9—C8	119.6 (3)
C1—O1—Ag1^{iii}	117.37 (19)	C10—C9—H9	120.2
C1—O1—Ag1^{v}	120.41 (18)	C8—C9—H9	120.2
Ag1^{iii}—O1—Ag1^{v}	88.24 (7)	C9—C10—C11	118.3 (3)
C1—O2—Ag1	143.8 (2)	C9—C10—H10	120.8
O3—O3—S1	0 (10)	C11—C10—H10	120.8
C3—N1—S1	130.8 (2)	C12—C11—C10	123.1 (3)
C3—N1—H1N	110.5	C12—C11—N2	118.9 (3)
S1—N1—H1N	118.1	C10—C11—N2	117.9 (3)
O5—N2—O6	124.1 (3)	C11—C12—C13	118.5 (3)
O5—N2—C11	118.6 (3)	C11—C12—H12	120.8
O6—N2—C11	117.3 (3)	C13—C12—H12	120.8
O2—C1—O1	124.2 (3)	C8—C13—C12	119.3 (3)
O2—C1—C2	118.6 (3)	C8—C13—H13	120.4
O1—C1—C2	117.3 (3)	C12—C13—H13	120.4

O4—S1—O3—O3	0.0 (6)	C4^{vi}—C5—C6—Ag1	92.3 (3)
N1—S1—O3—O3	0.0 (6)	C5—C6—C7—C2^{vi}	−0.2 (4)
C8—S1—O3—O3	0.0 (6)	Ag1—C6—C7—C2^{vi}	−86.7 (3)
O3—S1—N1—C3	−174.6 (3)	O3—S1—C8—C13	142.3 (2)
O3—S1—N1—C3	−174.6 (3)	O3—S1—C8—C13	142.3 (2)
O4—S1—N1—C3	−44.4 (3)	O4—S1—C8—C13	10.5 (3)
C8—S1—N1—C3	71.3 (3)	N1—S1—C8—C13	−106.9 (3)
Ag1—O2—C1—O1	20.5 (5)	O3—S1—C8—C9	−38.1 (3)
Ag1—O2—C1—C2	−158.7 (2)	O3—S1—C8—C9	−38.1 (3)
Ag1^{iii}—O1—C1—O2	−16.2 (4)	O4—S1—C8—C9	−169.8 (2)
Ag1^{v}—O1—C1—O2	89.1 (3)	N1—S1—C8—C9	72.8 (3)
Ag1^{iii}—O1—C1—C2	163.05 (17)	C13—C8—C9—C10	1.4 (5)
Ag1^{v}—O1—C1—C2	−91.7 (3)	S1—C8—C9—C10	−178.3 (2)
O2—C1—C2—C7^{iv}	168.7 (2)	C8—C9—C10—C11	−0.3 (5)
O1—C1—C2—C7^{iv}	−10.6 (4)	C9—C10—C11—C12	−1.0 (5)
O2—C1—C2—C3	−9.4 (4)	C9—C10—C11—N2	177.8 (3)
O1—C1—C2—C3	171.3 (2)	O5—N2—C11—C12	164.6 (3)
S1—N1—C3—C4	15.8 (4)	O6—N2—C11—C12	−16.0 (4)

S1—N1—C3—C2	−165.0 (2)	O5—N2—C11—C10	−14.3 (4)
C7^{iv}—C2—C3—N1	178.6 (2)	O6—N2—C11—C10	165.1 (3)
C1—C2—C3—N1	−3.3 (4)	C10—C11—C12—C13	1.1 (5)
C7^{iv}—C2—C3—C4	−2.2 (4)	N2—C11—C12—C13	−177.7 (3)
C1—C2—C3—C4	175.9 (3)	C9—C8—C13—C12	−1.3 (5)
N1—C3—C4—C5^{iv}	179.9 (3)	S1—C8—C13—C12	178.4 (2)
C2—C3—C4—C5^{iv}	0.7 (4)	C11—C12—C13—C8	0.1 (5)
C4^{vi}—C5—C6—C7	1.7 (5)		

Symmetry codes: (i) −*x*+1, *y*+1/2, −*z*+1/2; (ii) *x*, *y*+1, *z*; (iii) −*x*+1, *y*−1/2, −*z*+1/2; (iv) *x*, −*y*+3/2, *z*−1/2; (v) *x*, *y*−1, *z*; (vi) *x*, −*y*+3/2, *z*+1/2.

Hydrogen-bond geometry (Å, º)

D—H···*A*	*D*—H	H···*A*	*D*···*A*	*D*—H···*A*
C5—H5···O3	0.93	2.65	3.457 (4)	145
C13—H13···O5^{vii}	0.93	2.7	3.424 (4)	136
C12—H12···O6^{viii}	0.93	2.49	3.369 (4)	157
N1—H1*N*···O2	0.85	1.85	2.602 (3)	146
C4—H4···O4	0.93	2.41	3.062 (4)	127

Symmetry codes: (vii) *x*, −*y*+1/2, *z*−1/2; (viii) −*x*, −*y*, −*z*.